Published in final edited form as:
Nano Lett. 2012 April 11; 12(4): 1996–2002. doi:10.1021/nl2045952.

Aerosol Synthesis of Cargo-Filled Graphene Nanosacks

Yantao Chen[1], **Fei Guo**[2], **Ashish Jachak**[3], **Sang-Pil Kim**[2], **Dibakar Datta**[2], **Jingyu Liu**[1], **Indrek Kulaots**[2], **Charles Vaslet**[3], **Hee Dong Jang**[5,6], **Jiaxing Huang**[5], **Agnes Kane**[3,4], **Vivek B. Shenoy**[2,4,*], and **Robert H. Hurt**[2,4,*]

[1]Dept. of Chemistry, Brown University, Providence, Rhode Island [2]School of Engineering, Brown University, Providence, Rhode Island [3]Dept. of Pathology and Laboratory Medicine, Brown University, Providence, Rhode Island [4]Institute for Molecular and Nanoscale Innovation, Brown University, Providence, Rhode Island [5]Dept. of Materials Science and Engineering, Northwestern University, Evanston, Illinois [6]Department of Industrial Materials Research, Korea Institute of Geoscience and Mineral Resources, Yuseong-gu, Daejeon 305-350, Korea

Abstract

Water microdroplets containing graphene oxide and a second solute are shown to spontaneously segregate into sack-cargo nanostructures upon drying. Analytical modelling and molecular dynamics suggest the sacks form when slow-diffusing graphene oxide preferentially accumulates and adsorbs at the receding air-water interface, followed by capillary collapse. Cargo-filled graphene nanosacks can be nanomanufactured by a simple, continuous, scalable process and are promising for many applications where nanoscale materials should be isolated from the environment or biological tissue.

Keywords

graphene; graphene oxide; encapsulation; folding; core-shell structures; biocompatibility

Graphene oxide (GO) is a promising giant molecular precursor for the creation of new carbon materials, because it can be assembled in the colloidal state into complex two- or three-dimensional structures, and then reduced to carbon.[1-4] There is potential to systematically design these carbon architectures based on fundamental understanding of graphene/GO alignment, stacking, folding, wrinkling, scrolling, and interfacial adsorption.[5-24] There is a particular interest in graphene wrapping for nanocomposite materials,[4,25-27] where the wrapped component can be nanoparticles,[25-27] nanowires,[4,28] or bacteria.[29,30] The assembly mechanism is typically electrostatic attraction,[4,25,28] which requires surface chemical modification and pH control to achieve opposite charges; or covalent cross-linking,[4] which requires chemically specific surface modification. It has been recently reported that graphene oxide folds under the action of water surface tension during aerosol microdroplet drying to form crumpled graphene nanoparticles.[31,32] Aerosol microdroplet drying is a simple and scalable continuous nanomanufacturing process, and

*corresponding authors: Robert Hurt, School of Engineering, Box D, Brown University, Providence, RI 02912, Robert_Hurt@brown.edu, Tel: 401 863-2685, Vivek Shenoy, School of Engineering, Box D, Brown University, Providence, RI 02912, Vivek_Shenoy@brown.edu, Tel: 401 863-1475.

Supporting Information Available. GO characterization, data on irreversibility of folding, images of additional examples of filled nanosacks, results of early MD simulations, and confocal fluorescence microscopy images to confirm cellular uptake are provided. This material is available free of charge via the Internet at http://pubs.acs.org.

one of its attractive features is the potential to use multi-component feed solutions to fabricate composite materials with control of stoichiometry.

Here we show that monolayer graphene oxide can be co-suspended with a variety of second components in dilute aqueous phases and ultrasonically nebulized and dried/heated to produce nanoparticles that consist of electron transparent graphene "sacks" encapsulating an internal cargo. The filled graphene nanosacks are a self-assembled structure that occurs by spontaneous colloidal segregation of the sack and filler into a core-shell symmetry on the basis of differential diffusion rates and the tendency of GO to adsorb at the liquid-vapor interface. Inside the sacks, nanoparticle cargos can be isolated from the natural environment or from biological tissue, while still exhibiting useful photonic, magnetic, or radiological functions.

Graphene oxide was prepared by a modified Hummers method[33] and purified by a two-step acid-acetone wash to remove the salt byproducts.[34] To fabricate graphene nanosacks, 0.5 mg/ml suspensions of monolayer graphene oxide (1-2 μm lateral dimension) were ultrasonically aerosolized to produce a mist of 2 – 10 μm droplets suspended in a gas flow (0.8 lit/min nitrogen), which pass through an electrically heated furnace (70 – 600 °C) and are captured on porous polycarbonate filters. When graphene oxide is the only component in suspension, the products are crumpled graphene nanoparticles (Figure 1a) similar to those reported recently.[31,32] The particles are irregularly folded structures with mesopores (~ 4 nm, Figure 1f) likely associated with loop structures in the creased regions (Figure 1b,c). We observe that the 600 °C heated particles are stable after reintroduction into water – i.e. they do not dissolve or unfold.[31]

The crumpled nanoparticles can be made by heating, which reduces the GO precursor to an r-GO sack, or by dry-gas dilution at room temperature, which preserves the GO surface chemistry and insulating properties. In both cases, the microdroplet geometry allows fast drying, which we observe directly in the form of rapid disappearance of the mist phase within a few centimeters of the furnace entrance. Figure 1e gives estimates of drying times from a simple model of diffusion-limited evaporation from spherical microdroplets (see Supporting info). As long as the ratio of water/gas flow is low enough to prevent saturation from being reached, drying times are predicted to be short, 0.1 – 100 msec, in agreement with our observations, even at room temperature when dry gas dilution is used instead of heating. Figure 1d gives predictions of the distribution of GO layer number per microdroplet based on Poisson statistics. For droplets of 6 μm in diameter and a GO concentration of 0.5 mg/ml, one expects about 11 layers per droplet, which is consistent with the 10-15-layer packets seen in the walls of the crumpled nanoparticles by HRTEM (Figure 1c). The original suspension has a water-GO mass ratio of 2000:1, so the drying process is accompanied by a large size reduction and produces nanoscale structures from the starting microscale droplets.

To understand how binary suspensions assemble, we used hydrophilic, citrate-stabilized silver nanoparticles (AgNPs, 80 nm diameter) as a model water-dispersible second component. At low Ag-NP concentrations, the crumpled nanoparticle structure is preserved but the second component is found *inside* a thin graphene shroud (Figure 2a). At higher AgNP concentrations, we still see a graphene shroud (Figure 2b), but the graphene has fewer creases and opposing walls are no longer in contact. Instead, the structure resembles a sack with a cluster of Ag nanoparticles as contents. The filler appears to act as a scaffold that mechanically supports the graphene sack and prevents the complete collapse seen in Figure 1a. We then fabricated a series of sack-cargo materials by co-suspending GO with hydrophilic, aryl-sulfonated carbon black nanoparticles (Figure 2f), fluorescein-sodium dye (Figure S3c), DNA (Fig. S3d), and CsCl salt (Fig. S3e) all at high loadings (filler:GO mass ratio 2). In most cases, the sheets fully encapsulate the second component with no filler

material observed outside the nanosacks by SEM. If the chosen filler has a high atomic number (Ag, Cs), it can be directly visualized inside the sack by SEM (Figure 2a, b). Organic or carbon-based fillers are not easily observable, but their presence is reflected in the swollen sack structure (Figure 2f), and can be seen by TEM (Fig. S3b). Unlike other graphene wrapping methods that employ opposite surface charges to achieve electrostatic attraction[4,25,28], this method works best with cargos of the *same* charge (negative at neutral pH for GO, citrate-AgNPs, DNA, aryl-sulfonated-CB), which keeps both components in suspension stably without association until they are forced together by water surface tension in the late stages of drying.

As a test of encapsulation, we reintroduced the graphene-AgNP sack-cargo material (Fig. 2b) into pH 4 acetate buffer and measured the rate of silver ion release. Free Ag nanoparticles are known to react with dissolved oxygen and protons to liberate Ag^+,[36] and Figure 2e shows by direct comparison at equal dose of total Ag, that the sack covering greatly suppresses the corrosion reaction and associated ion release. The release of measurable Ag^+ suggests the nanosacks are not hermetically sealed, due either to defects in r-GO.[37,38], or to the presence of pores (Fig. 1f) that give access to the sack interior. We note that the barrier behavior of GO and rGO films is complex,[39] and more work is needed to fully characterize the barrier properties of nanosacks as a function of thickness and degree of reduction.

We become interested in the self-assembly mechanism that determines nanosack structure, which appears to be general and chemically non-specific. In previous work,[6] we observed that GO collects on the outer surfaces of water droplets as they dry, forming multilayer GO surface films or "skins" that wrinkle under compressive stress during droplet shrinkage. We also observe adsorption of graphene at the droplet-gas interface in our MD simulations (Fig. S4). We propose that two factors govern this surface film formation: (i) free energy reduction by interfacial adsorption of a monolayer sheet, and (ii) slow diffusion of the high-MW sheets, which allows additional sheets to be scavenged by the interface as the droplet surface recedes during drying (Fig. 3).

The thermodynamic driving force for graphene or GO interfacial adsorption is easily derived. The transfer of an ideal, infinitely thin sheet from the immersed state to the liquid-gas interface involves creation of a new solid-gas interface of energy, σ_s, and the destruction of an equal-area solid-liquid interface of energy σ_{sl} and an equal-area liquid-gas interface of energy, γ. In the absence of curvature (lateral sheet dimension ≪ droplet diameter), these contributions sum to the free energy change of adsorption:

$$\Delta G = \sigma_s \sigma_{sl} - \gamma \quad (1)$$

which can be rewritten using the Young equation ($\sigma_s = \sigma_{sl} + \gamma\cos\theta$) to yield:

$$\Delta G = \gamma(\cos\theta - 1) \quad (2)$$

which gives a negative (favorable) free energy change for all finite contact angles of water on the sheet material ($\theta > 0$). Water contact angles of GO have been reported to be 40 – 60°,[40-42] so there is a significant driving force for GO adsorption at the air-water interface of order 15-35 mJ/m^2. The existing of a driving force for GO interfacial adsorption is consistent with a number of literature observations that GO is amphiphilic and accumulates at the water-air interface[43-45] or water-oil interface.[7,43,46] Following monolayer adsorption, further sheets may gather by convective scavenging: the hydrodynamic radius of GO with 2 μm lateral dimension is about 750 nm using the disk model of Johnsson and Edwards,[47] from which the Stokes-Einstein diffusion coefficient, D, is 8×10^{-9} cm^2/s, giving a diffusive velocity, D/R, from the interface toward the interior of 8×10^{-5} cm/s. This is slow compared

to the motion of the drying front (~3×10^{-2} cm/s) so additional GO sheets will be readily collected (Figure 3). By this theory, when binary solution/suspension droplets dry, we anticipate GO will accumulate preferentially on the outside of the particle if two conditions are met: (i) the second component is water soluble or highly dispersible, and (ii) the second component diffuses faster than GO, and does not collect preferentially at the drying front. This is indeed the case for each of the second components studied here, and leads to the conceptual model of Figure 3. Note that statistically some GO sheets will be initially located near the center of the droplet, and being slow diffusers will not encounter the receding surface, and instead become a part of the core, imbedded with the cargo (see Fig. 2d). In the dilute suspensions used here, however, the volume reduction upon drying is large, and thus most GO layers do encounter the receding drop surface at some point, and contribute to the sack formation rather than the core.

For the rational development of nanosack technologies, we would like to better understand GO-water interactions and GO buckling, collapse, and creasing. For simplicity, we omit the filler phase, and consider the limiting case of empty nanosacks. Figure 4 shows selected images from molecular dynamics (MD) simulations of droplet drying in the presence of monolayer graphene (Figure 4a) and graphene oxide (Figure 4b) after an initial period where they first localize at the gas-water interface (Figure S4). We used the LAMMPS code,[48] and modeled the interatomic interactions with a reactive force-field (ReaxFF), which is a general bond-order-dependent potential that provides accurate descriptions of bond breaking and bond formation in hydrocarbon–oxygen systems.[49] This potential has been successfully used in other studies of graphene/water systems.[49-51] To manage the simulation size, we used 2000 H_2O molecules and a semi-2D graphene film of 130Å × 15Å with periodic boundary conditions in the Z direction. Graphene oxide structure is prepared by thermal annealing (T=1000K) of $C_{10}O_2(OH)_2$ structure, which is two epoxy and hydroxyl groups per 10 carbon atoms and distributed randomly on either side of the graphene basal plane.[51] The size of the simulation box is 150 Å ×100 Å ×15 Å, and charge transfer is performed by the charge equilibration (QEq) method[52] at every MD step. The temperature of the system is kept at 300K controlled by rescaling atomic velocities every 10 MD steps (each MD time step Δt=0.2 fs). To mimic drying, 10% of the H_2O molecules were randomly selected and removed every 5×10^4 fs.

The simulations predict very different behavior for graphene and graphene oxide during droplet drying (Figure 4). For graphene there is a noticeable gap at the water interface, and the droplet appears to template or “guide” the graphene into a scroll structure during drying. We believe that weak van der Waals forces in the water/graphene system[53] allow graphene to slide on the droplet surface, which enables this “guide and glide” assembly mode, similar to observations from previous simulations.[18] Graphene oxide in contrast appears to stick on the droplet surface and be dragged inward as the droplet volume is reduced by drying (“cling and drag” mechanism). Water-GO interactions are known to involve hydrogen bonding with oxygen-containing functional groups. We calculated attraction energies between a single water molecular and epoxy, carbonyl, and hydroxyl groups in our simulations as 0.30, 0.31, and 0.17 eV, respectively, typical of H-bonded interactions, and we believe these strong forces are responsible for the “cling and drag” assembly. Kinks appear early in the evolving graphene oxide structure and the end product is a crumpled and plastically deformed particle that bears strong resemblance to the collapsed sacks in Figure 1. Based on our analysis of the spatial distribution of functional groups (Figure S6) and the literature on folding behavior,[11,12] we suggest that the kink locations are initiated from sites of higher concentrations of functional groups or defects in the GO precursor (Fig. S6).

We were also interested in how the water-actuated folding process is influenced by layer number, droplet size, and surface chemistry, and under what range of conditions such folded

structures could be formed. A 2D analytical model was developed to describe the minimum energy configuration in the graphene/water-drop system as a function of extent of drying. The model begins with a single graphene sheet or multilayer stack adsorbed at the water-gas interface of a large droplet, which is the lower free energy starting state according to Equation (2). At each stage in the drying process, the system energy is the sum of terms for graphene curvature, liquid surface tension, and solid/gas and solid/liquid interfacial energies:

$$E=\frac{\kappa \cdot L}{2R_{GO}^2}+\gamma \cdot A_{H_2O-gas}+\sigma_{GO-gas} \cdot A_{GO-gas}+\sigma_{GO-H_2O} \cdot A_{GO-H_2O} \quad (3)$$

where γ is the surface tension of water, σ_{x-y}, A_{x-y} are the surface tension and contact area of x-y interface, L is the GO lateral dimension and R_{GO} is the radius of GO. Minimizing E gives a predicted curvature vs. droplet volume V. This is shown in Figure 4c-e, where the curvature is described not by R_{GO} directly, but by angle β (Figure 4c inset). Figure 4c shows how the initial bending and closing process depends on GO layer size. Single GO layers used in this study (1 – 2 μm lateral dimension) are easily bent to full closure (end state at β = 360°). Bending nanoscale GO, however, would involve high curvature, and below about 10 nm does not achieve full closure, but bends and then relaxes back to the planar state (see Figure 4c). This behavior is similar to that observed in our early MD simulations on small graphene segments (5 nm lateral dimension) interacting with water nanodroplets (Figure S5). Figure 4d shows the effect of stiffness, which is included primarily to understand the effect of layer number, N. Many practical graphene-based materials have multiple layers,[54] and in the absence of interlayer slippage the bending stiffness scales as N^3, and can reach 10^4 eV for a few-layer-graphene structure with 20 layers. Figure 4d shows that most few-layer-graphene materials at 2 μm lateral dimension can be water folded, but some multilayer structures may act as stiff plates under the action of water surface tension. Finally, Figure 4e shows the effect of contact angle. A contact angle of 40°, typical of GO, is only slightly more effective at layer bending than contact angles of 90°, typical of few-layer graphene. The modelling suggests that a wide range of graphene and GO structures can be manipulated by the weak forces of water surface tension.

We envision a broad set of technological uses for filled graphene nanosacks. Many potential applications derive from the ability of sacks to isolate nanoparticle cargos from biological tissue or the natural environment where uncontrolled particle release is undesirable due to human or ecological toxicity. In these cases, the sacks can passivate biological surface reactivity while allowing nanoparticle cargos to exhibit unique nanoscale functions such as superparamagneticity, size-dependent band-gaps and fluorescence, plasmon resonance, or can provide CT/MRI contrast enhancement. Potential applications lie in composite materials, electrodes, oxidation protection, magnetic theranostics and hyperthermia, electron imaging of volatile substances, and in vivo imaging probes. Sack leakage or biodegradation of GO as reported by Kotchey et al.[55] may allow delivery and controlled release applications. A number of studies use nanoscale GO as amphiphilic carriers of therapeutic agents[56-59] but the cargo load is limited by the geometric capacity of the material for molecular adsorption. Nanosack encapsulation is not limited by the geometric surface area of the carrier, and has been demonstrated here at cargo:GO ratios up to 200% (wt/wt).

Many biological applications will require biocompatibility. Figure 5 shows cell uptake and viability results for both the folded graphene NPs (empty nanosacks) and positive and negative nanoparticle controls. Human lung epithelial, H460, cells readily internalized the sacks within 24h (Fig. 5a), and the internal location was confirmed by confocal microscopy in the plane of the nucleus (Fig. S7). Nanosacks elicit a biological response similar to the

unfolded GO (Fig. 5b), and have low acute cytotoxicity at doses below 5 μg/ml, which makes them interesting candidates for further development in biomedicine.

Finally, we anticipate that nanosack applications will be facilitated by the simplicity and scalability of the fabrication method - it is a water-based continuous flow process related to industrial spray drying[9] that produces distinct uniform nanoparticles. It can use mild heating or even room temperature dry-gas dilution for thermally sensitive cargos. The generality of the assembly principle, the flexibility in composition, the ease of nanomanufacturing, and the increasing availability of the graphene oxide precursor are strong motivation for further development of graphene nanosack technologies.

Supplementary Material

Refer to Web version on PubMed Central for supplementary material.

Acknowledgments

The authors acknowledge financial support from the NSF Materials Research Science and Engineering Center at Brown, NSF grant CBET-1132446, the NIEHS Superfund Research Program grant P42 ES013660, NIEHS grant R01 ES016178, and the General Project of the Korea Institute of Geoscience and Mineral Resources (KIGAM) funded by the Ministry of Knowledge Economy of Korea. J.H. acknowledges support from the Alfred P. Sloan Foundation and NSF through a CAREER award (DMR 0955612).

References

1. Ruoff R. Nat Nanotechnol. 2008; 3:10–11. [PubMed: 18654440]
2. Lee SH, Kim HW, Hwang JO, Lee WJ, Kwon J, Bielawski CW, Ruoff RS, Kim SO. Angew Chem Int Ed. 2010; 49(52):10084–10088.
3. Lee SH, Lee DH, Lee WJ, Kim SO. Adv Funct Mater. 2011; 21(8):1338–1354.
4. Zhou W, Zhu J, Cheng C, Liu J, Yang H, Cong C, Guan C, Jia X, Fan HJ, Yan Q, Li CM, Yu Ting. Energy Eniron Sci. 2011; 4:4954–4961.
5. Compton OC, Nguyen ST. Small. 2010; 6(6):711–723. [PubMed: 20225186]
6. Guo F, Kim F, Han TH, Shenoy VB, Huang J, Hurt RH. ACS Nano. 2011; 5(10):8019–8025. [PubMed: 21877716]
7. Guo P, Song H, Chen X. J Mater Chem. 2010; 20:4867–4874.
8. Cote LJ, Kim F, Huang J. J Am Chem Soc. 2009; 131(3):1043–1049. [PubMed: 18939796]
9. Zhou X, Wang F, Zhu Y, Liu Z. J Mater Chem. 2011; 21:3353–3358.
10. Meyer JC, Geim AK, Katsnelson MI, Novoselov KS, Booth TJ, Roth S. Nature. 2007; 446:60–63. [PubMed: 17330039]
11. Schniepp HC, Kudin KN, Li J, Prud'homme RK, Car R, Saville DA, Aksay IA. ACS Nano. 2008; 2(12):2577–2584. [PubMed: 19206294]
12. Schniepp HC, Li J, McAllister MJ, Sai H, Herrera-Alonso M, Adamson DH, Prud'homme RK, Car R, Saville DA, Aksay IA. J Phys Chem B. 2006; 110(17):8535–8539. [PubMed: 16640401]
13. Xu Z, Buehler MJ. ACS Nano. 2010; 4(7):3869–3876. [PubMed: 20597529]
14. Cranford S, Sen D, Buehler MJ. Appl Phys Lett. 2009; 95:123121.
15. Li YF, Yu HQ, Li H, An CG, Zhang K, Liew KM, Liu XF. J Phys Chem C. 2011; 115(14):6229–6234.
16. Bellido EP, Seminario JM. J Phys Chem C. 2010; 114(51):22472–22477.
17. Kim K, Lee Z, Malone BD, Chan KT, Aleman B, Regan W, Gannett W, Crommie MF, Cohen ML, Zettl A. Phys Rev B. 2011; 83:245433.
18. Patra N, Wang B, Kral P. Nano Lett. 2009; 9(11):3766–3771. [PubMed: 19852466]
19. Cote LJ, Kim J, Zhang Z, Sun C, Huang J. Soft Matter. 2010; 6:6096–6101.

20. Behabtu N, Lomeda JR, Green MJ, Higginbotham AL, Sinitskii A, Kosynkin DV, Tsentalovich D, Parra-Vasquez ANG, Schmidt J, Kesselman E, Cohen Y, Talmon Y, Tour JM, Pasquali M. Nat Nanotechnol. 2010; 5:406–411. [PubMed: 20512130]
21. Kim JE, Han TH, Lee SH, Kim JY, Ahn CW, Yun JM, Kim SO. Angew Chem Int Ed. 2011; 50(13):3043–3047.
22. Xu Z, Gao C. ACS Nano. 2011; 5(4):2908–2915. [PubMed: 21375309]
23. Guo F, Mukhopadhyay A, Sheldon BW, Hurt RH. Adv Mater. 2011; 23(4):436.
24. Kim J, Cote LJ, Kim F, Huang J. J Am Chem Soc. 2010; 132(1):260–267. [PubMed: 19961229]
25. Yang S, Feng X, Ivanovici S, Mullen K. Angew Chem Int Ed. 2010; 49(45):8408–8411.
26. Zhu M, Chen P, Liu M. ACS Nano. 2011; 5(6):4529–4536. [PubMed: 21524132]
27. Cassagneau T, Fendler JH. J Phys Chem B. 1999; 103(11):1789–1793.
28. Han TH, Lee WJ, Lee DH, Kim JE, Choi E, Kim SO. Adv Mater. 2010; 22(18):2060–2064. [PubMed: 20352629]
29. Akhavan O, Ghaderi E, Esfandiar A. J Phys Chem B. 2011; 115(19):6279–6288. [PubMed: 21513335]
30. Mohanty N, Fahrenholtz M, Nagaraja A, Boyle D, Berry V. Nano Lett. 2011; 11(3):1270–1275. [PubMed: 21271738]
31. Luo J, Jang HD, Sun T, Xiao L, He Z, Katsoulidis AP, Kanatzidis MG, Gibson JM, Huang J. ACS Nano. 2011; 5(11):8943–8949. [PubMed: 21995602]
32. Ma X, Zachariah MR, Zangmeister CD. Nano Lett. in press.
33. Hummers WS, Offeman RE. J Am Chem Soc. 1958; 80(6):1339–1339.
34. Kim F, Luo J, Cruz-Silva R, Cote LJ, Sohn K, Huang J. Adv Funct Mater. 2010; 20(17):2867–2873.
35. Lastoskie C, Gubbins KE, Quirke N. J Phys Chem. 1993; 97(18):4786–4796.
36. Liu J, Sonshine DA, Shervani S, Hurt RH. ACS Nano. 2010; 4(11):6903–6913. [PubMed: 20968290]
37. Bagri A, Mattevi C, Acik M, Chabal YJ, Chhowalla M, Shenoy VB. Nature Chem. 2010; 2:581–587. [PubMed: 20571578]
38. Erickson K, Erni R, Lee Z, Alem N, Gannett W, Zettl A. Adv Mater. 2010; 22(40):4467–4472. [PubMed: 20717985]
39. Nair RR, Wu HA, Jayaram PN, Grigorieva IV, Geim AK. Science. 2012; 335(6067):442–444. [PubMed: 22282806]
40. Hasan SA, Rigueur JL, Harl RR, Krejci AJ, Gonzalo-Juan I, Rogers BR, Dickerson JH. ACS Nano. 2010; 4(12):7367–7372. [PubMed: 21114272]
41. Moon K, Lee J, Ruoff RS, Lee H. Nat Commun. 2010; 1(No.73)
42. Cote LJ, Cruz-Silva R, Huang J. J Am Chem Soc. 2009; 131(31):11027–11032. [PubMed: 19601624]
43. Kim J, Cote LJ, Kim F, Yuan W, Shull KR, Huang J. J Am Chem Soc. 2010; 132(23):8180–8186. [PubMed: 20527938]
44. Krueger M, Berg S, Stone D, Strelcov E, Dikin DA, Kim J, Cote LJ, Huang J, Kolmakov A. ACS Nano. 2011; 5(12):10047–10054. [PubMed: 22103932]
45. Chen C, Yang Q, Yang Y, Lv W, Wen Y, Hou P, Wang M, Cheng H. Adv Mater. 2009; 21(29): 3007–3011.
46. Kim F, Cote LJ, Huang J. Adv Mater. 2010; 22(17):1954–1958. [PubMed: 20432227]
47. Johnsson M, Edwards K. Biophys J. 2003; 85(6):3839–3847. [PubMed: 14645073]
48. Plimpton S. J Comput Phys. 1995; 117(1):1–19.
49. Chenoweth K, van Duin ACT, Goddard WA. J Phys Chem A. 2008; 112(5):1040–1053. [PubMed: 18197648]
50. Bagri A, Mattevi C, Acik M, Chabal YJ, Chhowalla M, Shenoy VB. Nat Chem. 2010; 2:581–587. [PubMed: 20571578]
51. Medhekar NV, Ramasubramaniam A, Ruoff RS, Shenoy VB. ACS Nano. 2010; 4(4):2300–2306. [PubMed: 20380417]

52. Rappe AK, Goddard WA. J Phys Chem. 1991; 95(8):3358–3363.
53. Leenaerts O, Partoens B, Peeters FM. Phys Rev B. 2009; 79(23):235440.
54. Sanchez VC, Jachak A, Hurt RH, Kane AB. Chem Res Toxicol. in press.
55. Kotchey GP, Allen BL, Vedala H, Yanamala N, Kapralov AA, Tyurina YY, Klein-Seetharaman J, Kagan VE, Star A. ACS Nano. 2011; 5(3):2098–2108. [PubMed: 21344859]
56. Bao H, Pan Y, Ping Y, Sahoo NG, Wu T, Li L, Li J, Gan LH. Small. 2011; 7(11):1569–1578. [PubMed: 21538871]
57. Liu K, Zhang J, Cheng F, Zheng T, Wang C, Zhu J. J Mater Chem. 2011; 21:12034–12040.
58. Liu Z, Robinson JT, Sun X, Dai H. J Am Chem Soc. 2008; 130(33):10876–10877. [PubMed: 18661992]
59. Bong JH, Compton OC, An Z, Eryazici I, Nguyen ST. ACS Nano. in press.
60. Pietruska JR, Liu X, Smith A, McNeil K, Weston P, Zhitkovich A, Hurt R, Kane AB. Toxicol Sci. 2011; 124(1):138–148. [PubMed: 21828359]

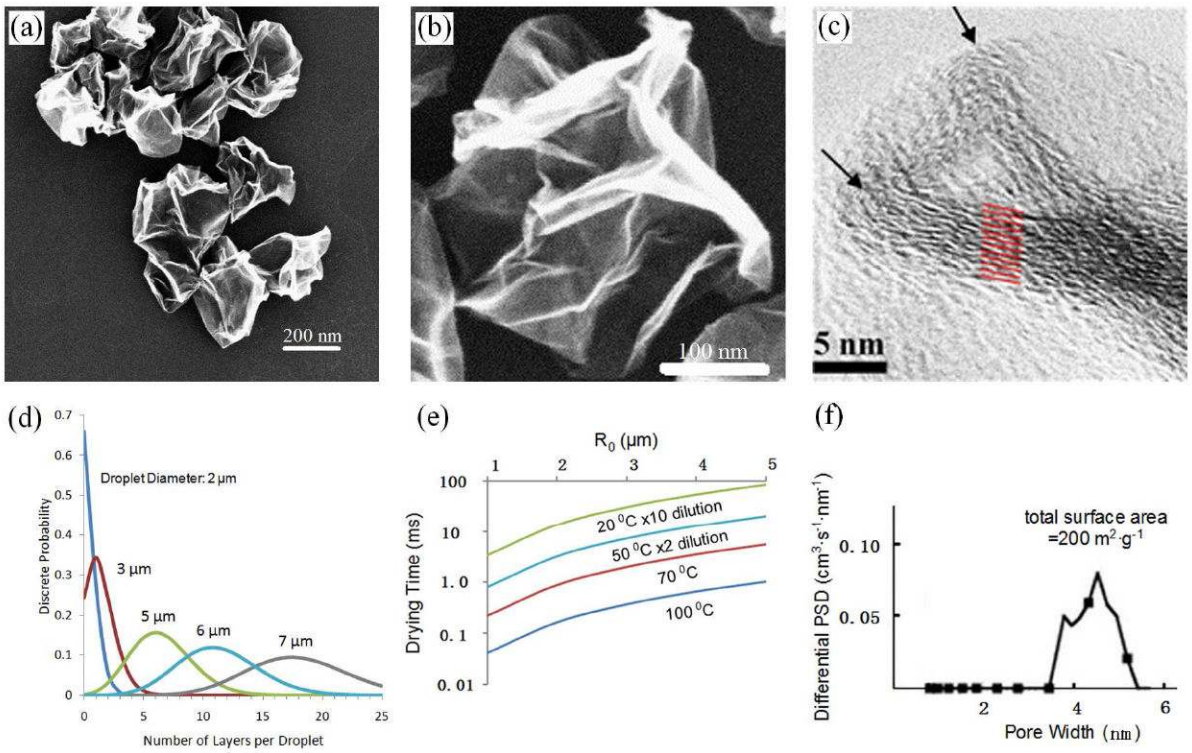

Figure 1.

Crumpled graphene nanoparticles fabricated by continuous microdroplet drying of colloidal GO suspensions. (a, b) SEM images showing folded sheet structure and extended creases, whose sharp edges suggest plastic deformation; (c) HRTEM showing multilayer structure (n ~ 12 layers) and discontinuous curvature (kinks) in the crease region; (d) Estimation of layer number per droplet/particle for a Poisson spatial distribution of GO sheets with 2 μm lateral dimension; (e) Calculated drying times showing the ability to fabricate the particles at very low temperature using dry gas dilution; (f) Pore size distribution determined by the NLDFT slit pore kernel[35] applied to nitrogen vapor adsorption isotherms showing a characteristic mesopore size of 3 - 5 nm, likely associated with the internal loops in the creases (see "c").

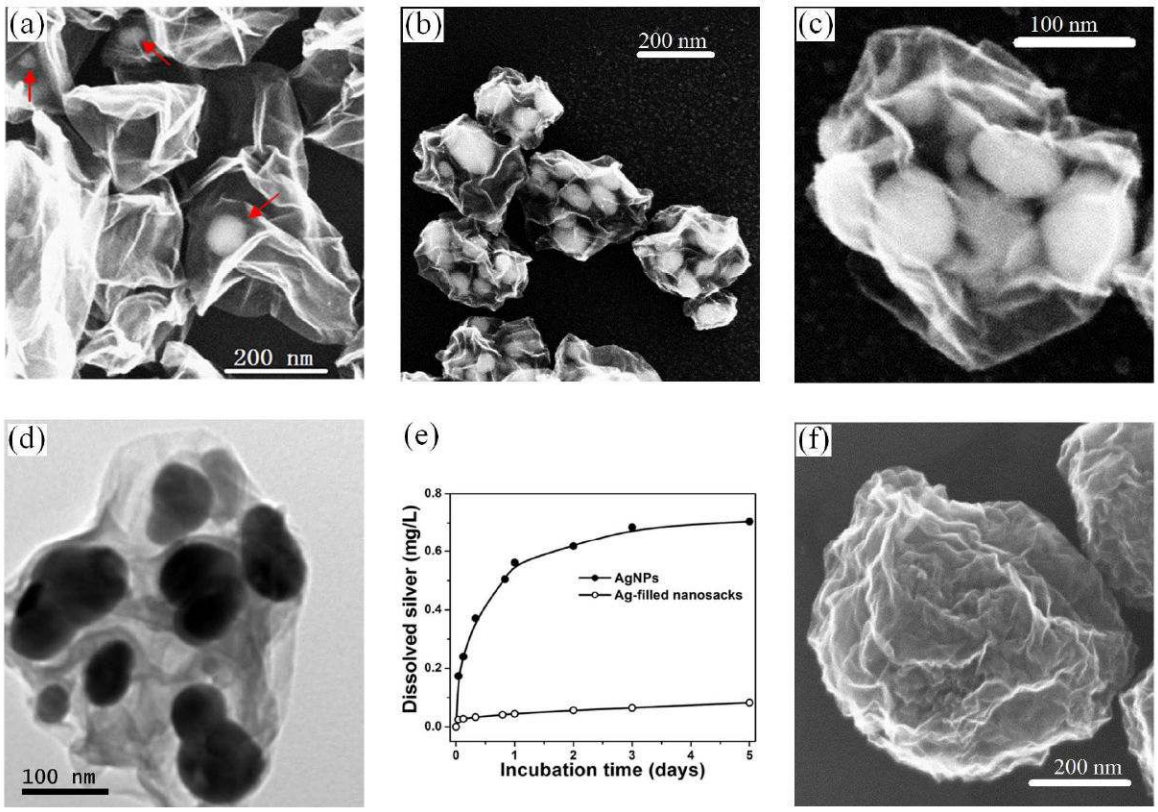

Figure 2.

Filled graphene nanosacks from drying binary microdroplet suspensions. (a) SEM of Ag-nanoparticle-filled sacks at low loading (Ag:GO mass ratio 0.06); (b,c,d) SEM/TEMs of silver nanoparticles at higher loading (Ag:GO mass ratio 2); (e) Time-resolved release of Ag^+ in 5 mM pH 4 acetate buffer from gradual oxidation of encapsulated nano-silver particles, vs. free Ag nanoparticle control. The sacks greatly inhibit Ag^+ release, and control experiments demonstrate the effect is not due to Ag^+ adsorption on GO functional groups, but rather to encapsulation. Concentrations measured by atomic absorption[36] at a common Ag dose of 2.6 mg/L; (f) hydrophilic, aryl-sulfonated carbon black (CB) nanoparticles at high loading (CB:GO ratio 2).

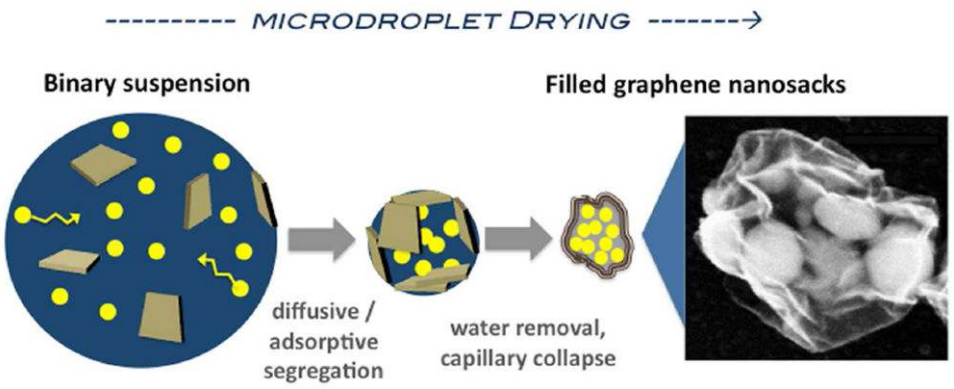

Figure 3.

Conceptual model for the colloidal self-assembly of filled graphene nanosacks. Microdroplet drying leads to graphene oxide adsorption and scavenging at the receding gas-water interface and partial segregation from the followed by sack closure and collapse by capillary forces. High filler loading acts as a scaffold to prevent complete sack collapse.

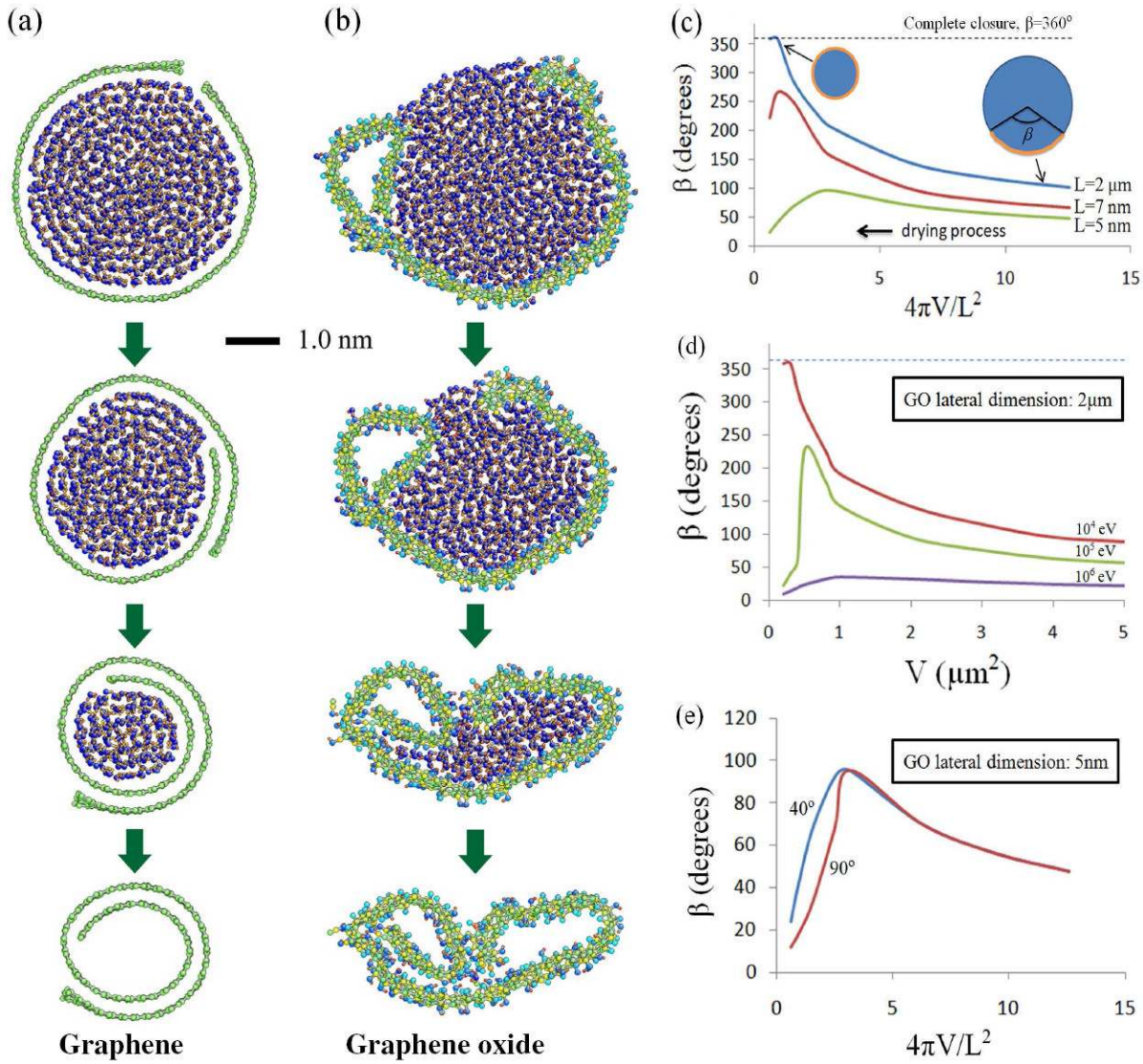

Figure 4.

Mechanisms of nanosack formation. (a,b) Molecular dynamics simulations of water-droplet-actuated scrolling, folding, or collapse for (a) monolayer graphene, which scrolls through a "guide and glide" mechanism; (b) Monolayer GO which closes and collapses by a "cling and drag" mechanism; (c-e) 2D analytical modeling of the early-stage droplet-actuated bending and closing process plotted as graphene curvature angle, β vs. droplet volume V or dimensionless drop volume $4\pi V/L^2$, where L is the lateral sheet dimension. (c) Bending and closing behavior as a function of GO lateral dimension. Bending to full closure is predicted to occur for the GO structures studied here, consistent with observations, but does not occur for nanoscale GO (< 10 nm lateral dimension) due to the high energy penalty for curvature at that length scale; (d) Bending as function of stiffness as determined by layer number in multilayer structures. At very high stiffness, the layers begin to fold (β increases) but then relax back to the planar state; (e) Bending as function of contact angle, which is a function of graphene oxidation state.

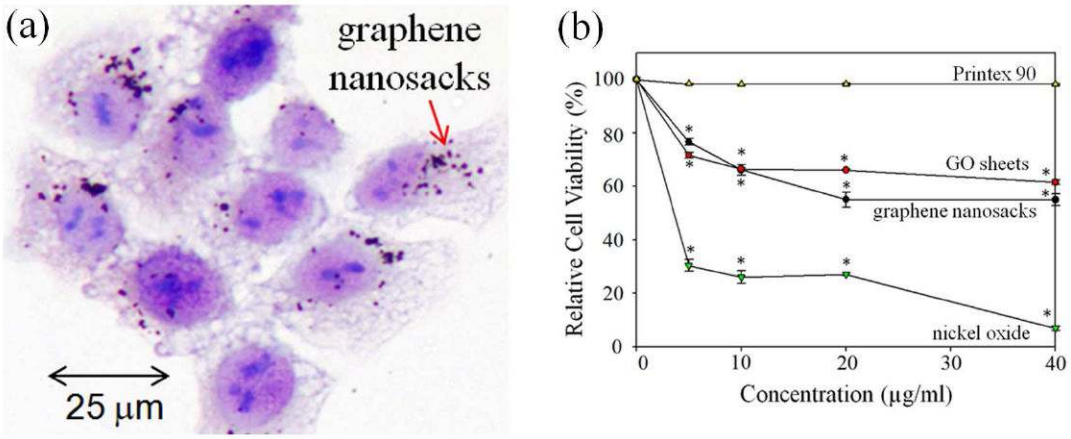

Figure 5.

Cellular response to graphene nanosacks. (a) Image of nanosacks localized in the cytoplasm 24 hr after exposure, May-Grünwald-Giemsa stain, light microscopy, 400× (b) viability of human lung epithelial cells 48 hr after exposure to graphene nanosacks and control samples including monolayer GO as sack precursor, nickel oxide nanoparticles[60] (<100 nm) as positive control for toxicity, and carbon black nanoparticles (Printex 90, primary particle size, 14 nm) as a negative toxicity control. Nanosacks show a similar dose-response curve to the plate-like GO precursor. Cell viabilities lie between those for the established positive and negative control samples and show low toxicity below 5 μg/ml. Statistical significance is indicated at *, $p < 0.05$ using a standard student's t-test.